Carbon 118 (2017) 467–474

Contents lists available at ScienceDirect

Carbon

journal homepage: www.elsevier.com/locate/carbon

Intrinsic mechanical properties of graphene oxide films: Strain characterization and the gripping effects

Enlai Gao [a, 1], Yeye Wen [b, 1], Yanan Yuan [a], Chun Li [b, **], Zhiping Xu [a, *]

[a] Applied Mechanics Laboratory, Department of Engineering Mechanics, Center for Nano and Micro Mechanics, Tsinghua University, Beijing 100084, China
[b] Department of Chemistry, Tsinghua University, Beijing 100084, China

ARTICLE INFO

Article history:
Received 3 February 2017
Received in revised form
22 March 2017
Accepted 25 March 2017
Available online 27 March 2017

ABSTRACT

Graphene oxide films are excellent structural and functional materials for their outstanding performance. Recent measurements reported widely scattered mechanical properties, which have been attributed to the difference in the chemistry and complex microstructures that rely on the fabrication process. In this work, we present an experimental study showing that the procedure of mechanical characterization is also critical for measuring intrinsic mechanical properties of graphene oxide films. We find that the specimen geometry and loading conditions could lead to significant variation in the measured stress, strain and toughness. To quantify these effects, we propose a rigid-plasticity shear-lag model to capture the effect of interfacial slippage at gripping ends, which can not only eliminate artifacts in measurements, but also be used to determine interfacial mechanical properties of gripping. Effects of grip pressure, length and loading rate are also discussed, following which suggestions for the experimental setup are provided. These understandings lay the ground for probing intrinsic mechanical properties of graphene oxide films in a reliably way.

1. Introduction

With emerging low-dimensional materials and technological development of synthesis and processing techniques, nanostructured assemblies in forms of films and fibers have been found wide applications as structural and functional components in relevant applications [1–6]. Building blocks and microstructures are the key information encoded into the macroscopic assemblies, which could be tuned to control the material performance [7–12]. Considering the outstanding mechanical properties of graphene, such as its tensile stiffness (1 TPa), strength (120 GPa) and resilience (20% strain to failure) [13–17], one would expect the films and fibers assembled in the layer-by-layer fashion to exhibit superior mechanical performance. Graphene oxide (GO), a hydrophilic derivative of pristine graphene, which assembles in the solvated phase, holds great promise in this scenario. GO films and fibers fabricated from their dispersions via vacuum-assisted filtration [1], evaporation induced self-assembly [18], electrospray coating [19], or wet spinning techniques [20] demonstrate impressive mechanical performance, including tensile stiffness of 6.8 GPa and 5.4 GPa, strength of 453 and 102 MPa and strain to failure up to 5.6% and 10.1%, respectively [21,22]. However, it should be remarked here that the performance reported for these materials in the literature is highly scattered, which has been attributed to the variation in the chemistry of GO sheets [23,24], and the microstructures that depend on the film or fiber forming process [20]. Moreover, one should be noted that due to the limitation in fabrication processes, the geometry of GO films is quite special, and may have significant impacts on the measurement for their high mechanical resistance.

The American Standard Test Method (ASTM) D882 is issued for mechanical tests of thin sheets under tension, which report the elongation, Young's modulus, tensile strength and strain to failure [25]. The ASTM D882 is designed for thin sheets with a length of ~100 mm and a thickness below ~1 mm to minimize the effects of interfacial sliding between grips. Accordingly, this can be done for GO films in practice by specifying the specimen geometry and validated further by quantifying the slippage at gripping ends and stress distribution in stretched sample. However, GO films prepared using current technology can hardly conform to the requirements declared in ASTM D882. Specifically, GO films fabricated via

* Corresponding author.
** Corresponding author.
E-mail addresses: chunli@mail.tsinghua.edu.cn (C. Li), xuzp@tsinghua.edu.cn (Z. Xu).
[1] These two authors contribute equally to this work.

http://dx.doi.org/10.1016/j.carbon.2017.03.080
0008-6223/

vacuum filtration are limited in both the lateral size and thickness. In the typical laboratory setup, the lateral size is defined by the container that is usually on the order of 10 mm, while the thickness h is about 10 μm as defined by the filtration or evaporation process. Consequently, slippage or shear in grips may lead to significant interfacial displacement that is incorrectly counted in the tensile strain of sample, which is measured based on the grip-to-grip distance L, as called grip separation. This issue, however, has been overlooked in previous studies. Our literature survey shows that the geometry of GO specimen is widely dispersed (Fig. 1a). For example, the grip separation L and width W ranges mostly from 4 to 20 mm and 1–6 mm, with the thickness h from 1 to 40 μm [1,18,21,26–49]. The effects of the specimen geometry and loading conditions then have to be well elucidated for a reliable design of measurements and industrial applications of GO films, as the specification in current test standards needs to be adjusted according to the material properties. In this work, we carried out a set of uniaxial tensile tests to address these issues, following by model analysis that quantitatively clarifies the underlying mechanisms. Practical rules are then suggested for measurements of intrinsic mechanical properties for GO films. Interfacial mechanical properties of gripping interface are also discussed based on the model analysis and results from mechanical tests.

2. Materials and methods

2.1. GO film fabrication

GO sheets with an average lateral dimension of 23 μm were synthesized by a modified Hummers method from natural graphite at a relatively low oxidation temperature of 0 °C [50]. Natural graphite powder (325 mesh, 3.0 g) was dispersed in 70 mL concentrated sulfuric acid under constant stirring with a speed of 350 rpm at 0 °C. After stirring for 2 h, 9 g potassium permanganate was added slowly over a period of 2 h. The reaction mixture was kept stirring for addition 8 h under the temperature at 0 °C. Then, 150 mL water was slowly added to the reaction mixture over 6 h by a peristaltic pump. All the reaction process was strictly controlled at 0 °C. The final reaction mixture was poured into 100 mL ice-water mixture to terminate the reaction, followed by the addition of hydrogen peroxide (30% aqueous solution) under stirring until no gas escape from the dispersion. The mixture was then filtered and washed with diluted (3.7%) hydrochloric acid aqueous solution to remove the metal ions, followed by washing using ultrapure water. The resultant slurry was then dispersed in distilled water under mild magnetic stirring to form a GO suspension. The GO suspension was purified by dialysis for two weeks. After that, it was centrifuged repeatedly at 3000 rpm to remove non-exfoliated aggregations. Finally, the GO suspension was concentrated by centrifugation at 10,000 rpm for 1 h. The concentration is confirmed to be 7.40 mg mL^{-1} by weighting the drying solid from 1 mL concentrated GO dispersion.

We follow the facile dispersion-evaporation method by cast drying 7.4 mg mL^{-1} GO dispersions on a polystyrene petri dish under ambient condition, which could be easily peeled for further characterization. The evaporation process typically takes 3 days at 25 °C. Fig. S1a in Supplementary Information (SI) shows the GO film fabricated from the dispersion-evaporation process. Fig. S1b in SI shows the scanning electron microscope (SEM) images taken by Sirion 200 field emission SEM that operates at a voltage of 10 kV, where the layered microstructure is clearly visualized. The size distribution of GO nanosheet histogram is measured from the SEM images (Fig. S2a, SI). It implies that the GO nanosheets have an average lateral size of ~23 μm. AFM image indicates that the average thickness of GO nanosheets is ~1 nm, which is comparable to that of a GO monolayer (Fig. S2b, SI). The X-ray photoelectron spectroscopy (XPS) spectra of GO shows the presence of four type carbon atoms, C–C/C=C (284.8 eV), C–O (286.8 eV), C=O (287.8 eV) and O–C=O (289.0 eV), implying that several types of oxygenated groups are attached on to the GO sheet (Fig. S2c, SI). The Raman spectrum of GO flakes on the Si/SiO_2 substrate displays a D-band at 1348 cm^{-1} and a G-band at 1590 cm^{-1} (Fig. S2d, SI). The intensity ratio between the D- and G-band (I_D/I_G) is 1.97, indicating the structural integrity of GO nanosheets from the modified Hummers procedure carried out at a relatively low oxidation temperature of 0 °C.

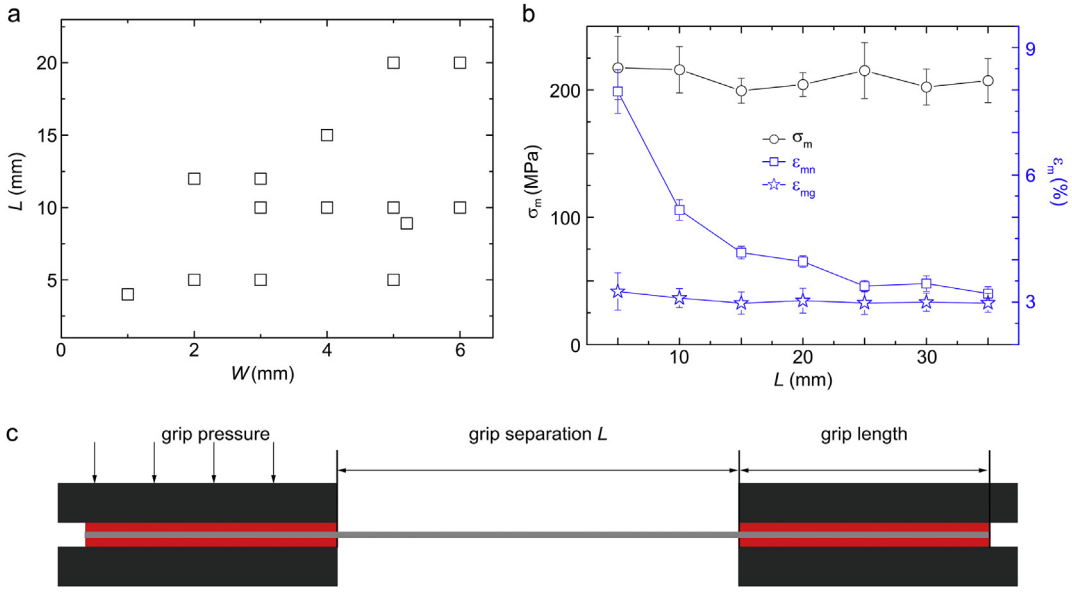

Fig. 1. (a) A literature survey on the geometry (length L, width W) of GO film specimen in previous studies [1,18,21,26–49]. (b) Stain to failure measured by the gauge and gripping methods, and the tensile strength determined for test specimens with different grip separation L. (c) The experimental setup of uniaxial tensile tests. (A colour version of this figure can be viewed online.)

2.2. Mechanical characterization

Uniaxial tension of GO films was carried out using an Instron 3342 universal testing machine (Instron, USA) (Fig. S3, SI). The grips of this machine have flat faces covered with thin rubber, which could apply a specified grip pressure through pneumatic fixture. The strain rate can also be controlled during the operation, with one gripping end moving while the other fixed.

All GO film samples were cut into rectangular strips by a razor blade. The width-to-thickness ratio is controlled to be on the order of 10^2, which satisfies ASTM-D882 that suggests a minimum ratio of 8 to achieve a uniform deformation in the strip even with the presence of inhomogeneous strain or flaws at the edges [25]. This is verified by the uniform deformation observed in the GO sample under tension (Fig. S4, SI). The grip length in the uniaxial tension is $l_g = 10$ mm to minimize the slippage of GO films, as validated by our experiments and RPSL model shown in Fig. 4a, and the grip separation L is chosen as 5, 10, 15, 20, 25, 30 and 35 mm to explore the gripping effect.

Tensile tests are performed at a uniaxial strain rate of 5×10^{-4} s^{-1}, corresponding to loading rates at 0.15, 0.30, 0.45, 0.60, 0.75, 0.90 and 1.05 mm min^{-1} for the specimen with different values of L, which has a minor effect on the stress and strain measurements as validated by results in Fig. 5b. To calculate the nominal stress, we use the initial cross-section area. Tensile stress in the sample is assumed to be uniform across the sample and its amplitude is calculated from the grip forces that are recorded by the testing machine. The strain in sample is measured by two different approaches. In the first so-called gripping method, we measure the nominal tensile strain ε_n from the change in L, that is ΔL, and then divided it by the original grip separation L, *i.e.*, $\varepsilon_n = \Delta L/L$. This method has been widely used in previous studies [1,21,29,30,46]. In the second so-called gauge method, we make gauge markers in the GO thin-film specimen that are selected from the optical feature points in images recorded during the tests using a digital camera (MER-500-7UC-L, 2592/Hx1944/W, 7 fps, Daheng Imaging, China). The tensile strain ε_g is then measured from the change ΔL_0 in the uniaxial gauge length between feature points in central region of the test specimen (Fig. S1a, SI), divided by its original value L_0, *i.e.*, $\varepsilon_g = \Delta L_0/L_0$. The experimental setup is shown in Fig. S3a. The time-series of sample images are analyzed by using the ImageJ software [51] to track the displacement of markers. Fig. S3b in SI shows a typical stress-strain relationship of GO films. All stress-strain data presented in this work are averaged over at least 5 GO strips with the same geometry. Most of the samples fail by crack nucleation at the central part (Fig. S4, SI). However, some tests reveal sliding failure at the interface with the grips, or fracture close to the grip ends, which are attributed to the poor gripping process and defects in the specimen. These results are not included for discussion.

To analyze the stress distribution in samples with different aspect ratio, we carry out the finite element method (FEM) based modeling on two specimen with sizes 5 mm × 3 mm and 30 mm × 3 mm, respectively. A two-dimensional plane-stress model with isotropic linearly elastic material properties is used. To probe the effects of gripping boundary conditions applied in experiments, the bottom boundary of samples are fixed while the top one is displaced upward for a stretch of 3%, and the spatial distributions of axial stress σ_y, the maximum principal stress and von Mises stress are summarized in Fig. S5, as normalized by the averaged axial stress.

To quantify the interfacial shear strength at grips, we design a test setup with asymmetric grips as illustrate in Fig. 2b. In this setup, the lengths of grips at two ends are made different so under a tensile load F, one end slides fully while the other bears elastic shear deformation only. Specifically, the grip length of GO films at one grip end is ~1 mm, while that at the other end is > 10 mm. The interfacial shear strength τ_s at the fully sliding end is $-k_1/(1 - k_1/k_2)/2W$, where k_1 and k_2 are the slopes of load and displacement curves measured by the testing machine (Fig. 2c).

3. Results and discussion

3.1. Geometry of the specimen

GO films are fabricated and characterized as reported in the previous work [21] (Fig. S1 and S2 in SI see also details in Materials and Methods). Under uniaxial tension, the GO films are stretched between the grips (Fig. S3, SI). Most of the samples we measured fail by initializing cracks in the central region, indicating that the interfacial load transfer between grips and the GO sample is sufficient and the force measured corresponds to the intrinsic stress level within the GO films. However, from optical images of deformed specimen (Fig. S4, SI), we notice that (1) there is prominent slippage at the interface between the GO film and grips, (2) the deformation in the GO sample, which is visualized through shining lines on its surface, is uniform in the central region. This uniform stress distribution is further validated by our finite element analysis (FEA) (Fig. S5, SI), which show that the derivation of stress amplitude from the averaged value, *i.e.* stress based on the uniform strain assumption of uniaxial tension, is below 5% for samples with lateral dimensions of 5 mm (L) × 3 mm (W), 30 mm (L) × 3 mm (W).

Based on the measurements, we summarize the tensile strength σ_m and strain to failure ε_m (ε_{mn} is the nominal strain to failure measured by the gripping method, while ε_{mg} is the strain to failure measured by the gauge method, see details in Materials and Methods) in Fig. 1b for samples with different grip separation L. For brittle materials with high concentration of imperfections, the weakest-link theory predicts a statistical size dependence of material strength [52]. However, our experimental results here show that at the length scale we probe in this work, this effect is minor. From the data collected, we find that the tensile strength of GO film does not change with L, suggesting sufficient load transfer into the samples. However, the maximum strain (strain to failure) ε_{mn} measured by the widely-used gripping method demonstrates prominent dependence on L. This artifact produced in the gripping method is reduced as L increases. This result indicates that the nominal strain to failure ε_{mn} recorded by the testing machine cannot characterize the intrinsic deformation of GO films with low L values. Instead, the interfacial sliding occurring in grips makes significant contribution to the displacement measured between loaded crossheads. In contrast, the strain to failure ε_{mg} measured by the gauge method and recorded with camera (see Materials and Methods) corrects this gripping effect, which displays gentle dependence on L and demonstrates its capability to quantify the intrinsic mechanical properties of GO samples in uniaxial tensile tests. Comparing the measured values of nominal strain to failure ε_{mn} and gauge strain to failure ε_{mg}, we find that ε_{mn} measured for samples with $L = 5$ mm is 7.96%, which is 266.9% higher than the intrinsic strain in the GO samples. As L increases to 25 and 35 mm, ε_{mn} is 3.44% and 3.20%, which then converges to the value ε_{mg} measured by the gauge method. It should be noted our GO films of which the sheet is produced by low temperature oxidation [21] exhibit higher failure strain than that reported in previous studies (1%) where the conventional procedure was adopted [1].

To quantify the gripping effect, *i.e.* the contribution of interfacial sliding to the measured nominal strain ε_n, we develop a theoretical model as illustrated in Fig. 1c. The stretch of GO specimen measured between the grips is $\varepsilon_n L$, which include the intrinsic elongation εL in

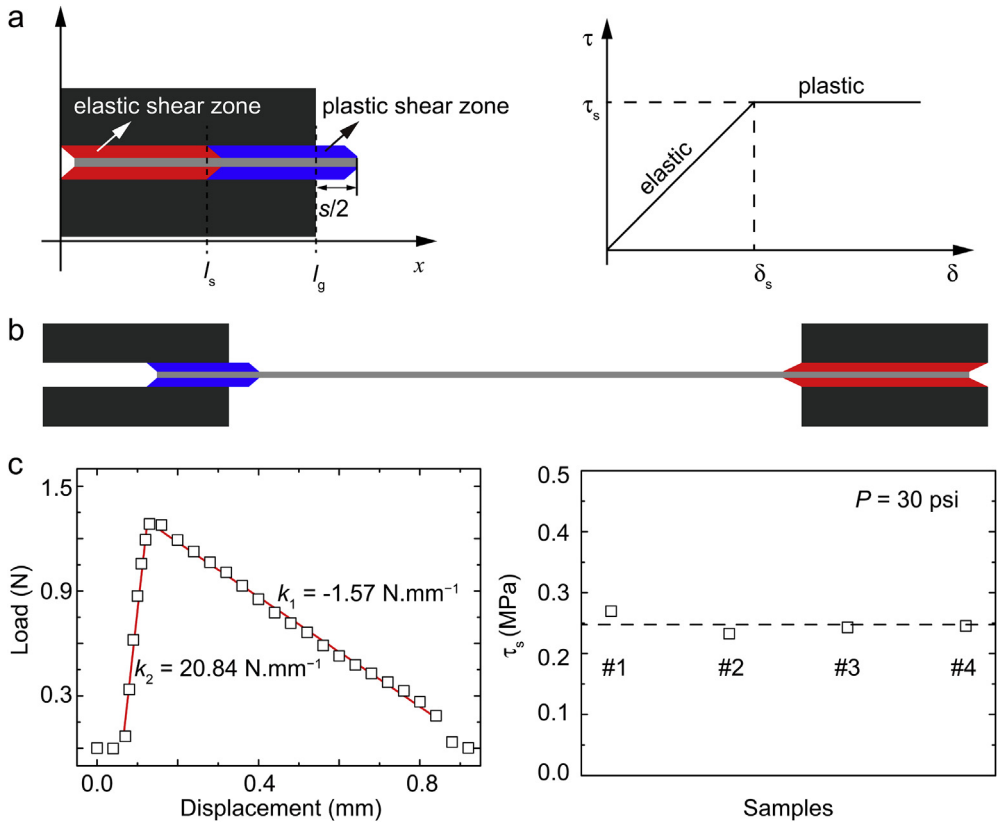

Fig. 2. (a) Elastic and plastic shear zones in the RPSL model and the interfacial constitutive relations between shear stress and shear displacement. (b) The experimental setup for mechanical characterization of the shear strength of gripping interface, with two asymmetric gripping ends. (c) A typical load-displacement curve measured for the interfacial slippage, from which the shear strength is determined to be $\tau_s = -k_1k_2/(k_2 - k_1)/2W$. The averaged value (the dash line) measured for four different samples at a gripping pressure of 30 psi is 0.248 MPa. (A colour version of this figure can be viewed online.)

the GO sample and the shear or slippage displacement s at two griping ends. As a result, ε_n is

$$\varepsilon_n = (\varepsilon L + s)/L = \varepsilon + s/L \quad (1)$$

Fitting our experimental data using Eq. (1) yields $s = 0.25$ mm for all samples, which is very close to the value $s = 0.23$ mm measured directly from optical images (Fig. S4). In consequence, Eq. (1) offers an accurate estimation of gripping-end slippage and intrinsic strain in the GO samples.

To elucidate the gripping effect more explicitly and extract key interfacial parameters from our experimental results, a rigid-plasticity shear-lag model (RPSL) is then proposed following the experimental setup (Fig. 2a). Although the tensile strain within a single GO sheet with lateral size of a few microns is spatially non-uniform due to the brick-and-motar topology of GO films [53], one could still assume the whole film to be uniform and isotropic in the loading plane considering the much larger size of samples (a few millimeters). Then the interfacial mechanical properties at gripping ends can be extracted from the load transfer or balance between shear at the interface and tension in the sample.

In our model, mechanical properties of the GO film are determined by fitting our experimental data into a linear elastic model (Fig. S3b, SI). For the sample with a width W of 3 mm and a thickness t of 9.73 μm, we obtain a tensile stiffness $D = 10^5$ N m^{-1} and the maximum tensile load $F_m = 2 \times 10^3$ N m^{-1} (per unit width) the film could bear, corresponding to a Young's modulus Y of 10.6 GPa ($Y = D/t$) and a tensile strength of $\sigma_m = 206$ MPa ($\sigma_m = F_m/t$) defined through the initial cross-section area, respectively. In our tests, the thickness decreases by ~18.6% before the film breaks, that is, Young's modulus of the GO film is overestimated if we use its thickness measured after tensile failure in the definition of Y, and thus these definitions based on the nominal stress reasonably capture the mechanical resistance of GO films (Fig. S6, SI).

In the RPSL model, the relation between shear stress $\tau(x)$ and displacement $\delta(x)$ at specimen-grip interfaces is assumed to be rigid-plastic, *i.e.*

$$\tau(x) = K\delta(x) \text{ for } \delta(x) \le \delta_s \text{ and } \tau(x) = \tau_s \text{ for } \delta(x) > \delta_s \quad (2)$$

Here K is the interfacial shear stiffness and δ_s is a critical displacement for the interfacial plastic deformation to be activated (Fig. 2a). The grips are far thicker than the GO film and thus its displacement can be neglected or considered as a part of the interfacial shear displacement. Our experimental results show that under a grip pressure of 30 psi, the shear strength is determined to be $\tau_s = 0.248$ MPa through measurements under a test setup with two asymmetric grips, which is designed specifically for measuring the interfacial shear strength (Fig. 2b and c, see Materials and Methods).

The equilibrium equation of RPSL model (Fig. 2a) for the materials in elastic shear zone ($0 \le x \le l_s$) is

$$D\mathrm{d}\delta^2(x)/\mathrm{d}x^2 = 2K\delta(x) \quad (3)$$

By denoting $F_1 = F - 2\tau_s(l_g - l_s)$, that is the tensile force in the specimen measured at the interface between elastic and plastic shear zones, we have the boundary conditions $D\mathrm{d}\delta(x)/\mathrm{d}x = F_1$ for $x = l_s$ and $D\mathrm{d}\delta(x)/\mathrm{d}x = 0$ for $x = 0$. The solution for shear displacement can then be determined as

$$\delta(x) = F_1 \cosh\beta x / D\beta \sinh\beta l_s, \quad \beta = (2K/D)^{1/2} \tag{4}$$

Now consider our experimental results in Fig. 1b. By assuming that the interface between the GO film and grips is under elastic shear (Fig. 1c), we will then have $l_s = l_g$ and $F_1 = F_m$. With the value of $\delta(l_g) = s/2 = 0.125$ mm determined from our experiments (Fig. 3a), we find $K = 1.46$ GPa m^{-1} from Eq. (4). In this situation, as the maximum shear displacement $\delta(l_g) = 0.125$ mm is smaller than the critical value $\tau_s/K = 0.17$ mm, we can confirm the assumption of elastic shear at the interface is valid for our experiments with $F \le F_m$.

However, taking into account for plastic shear is necessary in certain circumstances. For example, as a stronger GO film or for a weaker gripping interface is present, plastic shear, namely partial or full interfacial sliding, may occur, and thus the inelastic behavior has to be included in the RPSL (Eq. (2)). Specifically, the equilibrium equation for the plastic shear zone ($l_s < x < l_g$) can be written as

$$D\mathrm{d}\delta^2(x)/\mathrm{d}x^2 = 2\tau_s \tag{5}$$

Combined Eq. (5) with the boundary conditions $D\mathrm{d}\delta(x)/\mathrm{d}x = F_1$ for $x = l_s$ and $D\mathrm{d}\delta(x)/\mathrm{d}x = F$ for $x = l_g$, the solution for the shear displacement is

$$\delta(x) = \left[\tau_s x^2 + (F - 2\tau_s l_g)x + c\right]/D \tag{6}$$

The condition of continuity for $\delta(x)$ at $x = l_s$ is then

$$\delta(l_s) = F_1 \cosh\beta l_s / D\beta \sinh\beta l_s = \left[\tau_s l_s^2 + (F - 2\tau_s l_g) l_s + c\right]/D = \tau_s/K \tag{7}$$

From the governing Eqs. (4), (6) and (7) derived for the stress and strain in elastic and plastic shear zones, we can probe the slippage of GO films at grips and the evolution of gripping interface from elastic and plastic shear zones as loads increases. The results summarized in Fig. 3b show that at $F/F_m = 0.25$, 1.00 and 1.36, the shear deformation of gripping interface is fully elastic, and the length of elastic shear zone, l_s, keeps at a constant ($l_s = l_g$) and the shear displacement of GO films at grips, s, increases linearly with F. However, l_s decreases and s increases rapidly with F as F/F_m exceeds the critical value 1.36 when the plastic deformation occurs. At $F/F_m = 2.48$, the gripping interface fully develops into plastic shear and cannot resist further loads. In addition, we also could determine the shear and tensile stress distributions at gripping interfaces and within the whole GO film (Fig. 3c). These results clearly reveal stress and strain evolution in the tensile tests and demonstrate the impact of interfacial slippage on the experimental extraction of mechanical properties.

3.2. Suggestions for experimental setups

Based on the understandings of the gripping effect, we can now outline the guiding rules in designing mechanical tests for GO films. Specifically, the grip length l_g is the key adjustable factor. Our experimental results and RPSL model analysis suggest that a grip length larger than 10 mm is required to minimize the interfacial shear displacement to converge below ~0.25 mm (Fig. 4a). The effect of grip length is important but overlooked and scarcely mentioned in the literature where tensile tests of GO films were reported [16,43]. In practice, the grip length is limited by the size of GO films, and thus 10 mm would be an optimal minimum length for samples with typical sizes, stiffness and grip interfaces. To reveal the role of film-grip interface in modulating the load transfer and interfacial slippage, we tune the grip pressure P_g further in the tests. With the merit of our RPSL model, we are able to quantify the interfacial shear strength τ_s corresponding to a specific value of P_g. Our measurements show that τ_s increases with P_g. As P_g increases beyond 20 psi, the interfacial shear strength converges to a constant value of ~0.25 MPa (Fig. 4b), and higher pressure may destruct

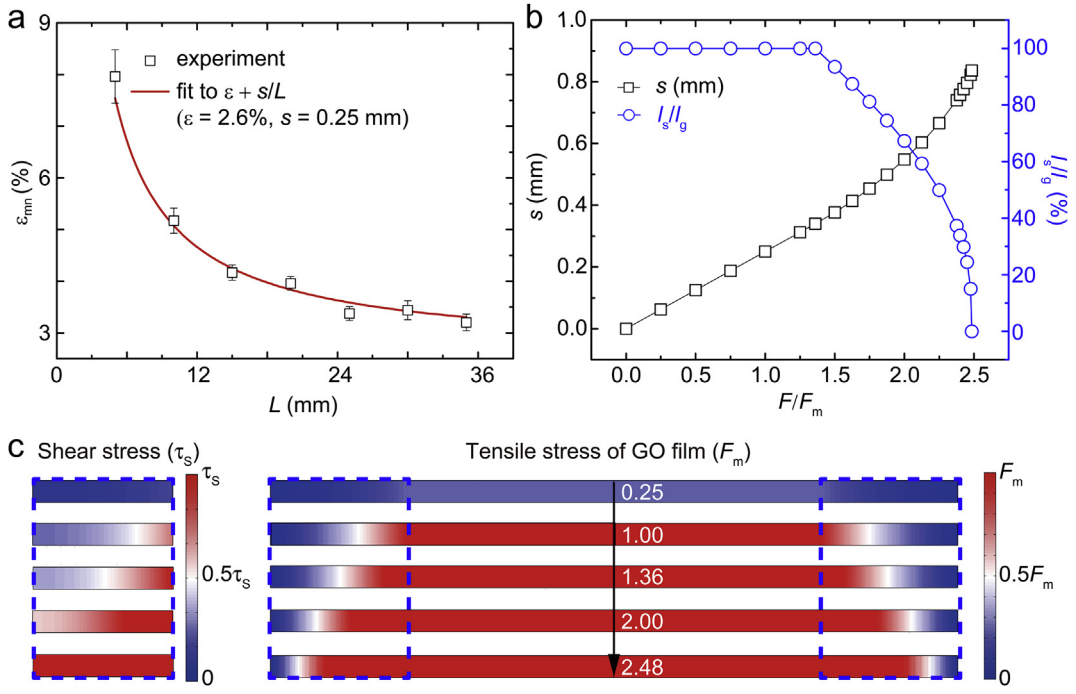

Fig. 3. (a) Fitting of experimental data of nominal strain to failure using Eq. (3). (b) The evolution of elastic, plastic shear displacements, and relative size of the elastic zone at the gripping interface with increasing load. (c) Distribution of interfacial shear stress and in-film tensile stress calculated from the RPSL model, demonstrating the activation of interfacial sliding as the amplitude of load increases. (A colour version of this figure can be viewed online.)

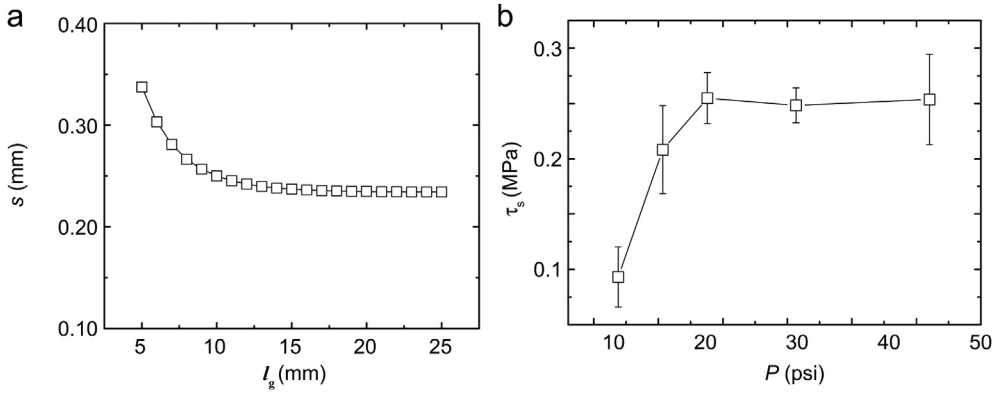

Fig. 4. (a) The shear displacement at the grip end with various grip length. (b) Shear strength of gripping interface measured under various grip pressure.

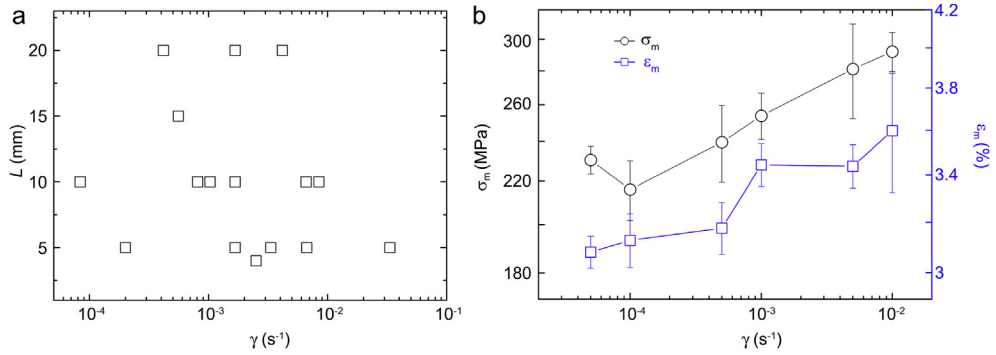

Fig. 5. (a) A literature survey on the grip separation L and uniaxial stretching rate used in previous mechanical tests [1,18,21,26–49]. (b) The loading-rate dependence of tensile strength and strain at failure for GO films. (A colour version of this figure can be viewed online.)

the GO sample that is unfavorable. Consequently, 20 psi is suggested as the optimal minimum grip pressure for the tests and is chosen in this work.

From our literature survey (Fig. 5a), most of previous studies adopt the strain rate r in the range between 10^{-4} and 10^{-2} s^{-1}. To clarify the loading-rate dependence, we carried out uniaxial tensile tests, and the results suggest that the tensile strength σ_m and strain to failure ε_m demonstrate very gentle variation in the range of $r = 5 \times 10^{-5} - 10^{-3}$ s^{-1} (Fig. 5b). However, the rate dependence becomes significant as r increases further, from 10^{-3} to the highest rate 10^{-2} s^{-1} we tested. The values of strength and strain to failure can be overestimated up to 135.2% and 115.1% at a high strain rate of 10^{-2} s^{-1} comparing that measured at a low strain rate of 10^{-4} s^{-1}. This loading-rate effect originates from the viscoelasticity of GO films manifested by their microstructural changes [54]. As a suggestion for minimizing the loading-rate dependence in practice, we suggest to adopt a strain rate below 10^{-3} s^{-1} as we did in this work.

3.3. Additional remarks on the stress distribution

There are three geometrical parameters for the samples and mechanical tests, including the width W, aspect ratio α of GO films and the grip separation L. The sample length controls the contribution of gripping slippage to the nominal strain measured in the tests, while the aspect ratio $\alpha = L/W$ determines the stress distribution that is affected by the gripping boundary condition. In our previous discussion on experimental data, the same width of 3 mm was used for all samples considering the fact that the strain distribution is spatially uniform, which, however, could be modified as the width changes. According to the Saint-Venant principle [55], inhomogeneity in the stress and strain distributions could occur for samples with a low aspect ratio that is defined as the ratio between grip separation L and width W. To probe this effect, we carried out FEA for two samples with two different sizes as chosen in our experiments, which are 5 mm (L) × 3 mm (W), 30 mm (L) × 3 mm (W), respectively (Fig. S6, SI). The maximum amplitude of derivation in stress from the averaged value is below 5% in the central region of GO films, where most material fracture is observed in the tensile tests.

We then explore the effect of sample width specifically by performing more tests. We cut the GO films with three different geometries using a template grid, with widths $W = 1$, 3 and 6 mm, respectively (Fig. S7a, SI). Our experimental results show that the tensile strength and strain to failure measured from the gripping method are independent on W (Fig. S7c, SI). It should be noted that the inaccuracy of the cutting process is ~0.08 mm, which leads to a relative error of 8% for $W = 1$ mm and 1.3% for $W = 6$ mm (Fig. S7b, SI). As a result, the width of GO film cannot be too small by considering this source of error. With the results from our tensile tests and FEA, we confirm that for the sample widths adopted by most experiments reported in the literature and this work has a minor effect on the tensile strength.

4. Conclusions

To conclude, we perform experimental measurements and theoretical analysis to reveal potential issues in measuring mechanical properties of GO films by uniaxial tensile tests. We find that the gripping effect can lead to significant overestimation of the strain measured from the grip separation and thus toughness of GO

films for specimen with low grip separation and grip length, which has been overlooked in previous studies. A theoretical model is proposed here to correct the gripping effect, which can also be used also to extract interfacial mechanical properties between the GO films and the grips. Besides of the geometrical effect, other considerations such as the grip pressure, loading rate are also discussed. Based on these understandings we outlined a practical guideline to measure intrinsic mechanical properties of GO films.

Acknowledgments

This work was supported by the National Natural Science Foundation of China through Grants 11222217 and 11472150 and 51673108. The computation was performed on the Explorer 100 cluster system of Tsinghua National Laboratory for Information Science and Technology.

Appendix A. Supplementary data

Supplementary data related to this article can be found at http://dx.doi.org/10.1016/j.carbon.2017.03.080.

References

[1] D.A. Dikin, S. Stankovich, E.J. Zimney, R.D. Piner, G.H. Dommett, G. Evmenenko, et al., Preparation and characterization of graphene oxide paper, Nature 448 (7152) (2007) 457–460.
[2] H. Chen, M.B. Müller, K.J. Gilmore, G.G. Wallace, D. Li, Mechanically strong, electrically conductive, and biocompatible graphene paper, Adv. Mater. 20 (18) (2008) 3557–3561.
[3] N. Behabtu, C.C. Young, D.E. Tsentalovich, O. Kleinerman, X. Wang, A.W. Ma, et al., Strong, light, multifunctional fibers of carbon nanotubes with ultrahigh conductivity, Science 339 (6116) (2013) 182–186.
[4] R.R. Nair, H. Wu, P.N. Jayaram, I.V. Grigorieva, A.K. Geim, Unimpeded permeation of water through helium-leak-tight graphene-based membranes, Science 335 (6067) (2012) 442–444.
[5] J. Lu, C. Cheng, Y. He, C. Lyu, Y. Wang, J. Yu, et al., Multilayered graphene hydrogel membranes for guided bone regeneration, Adv. Mater. 28 (21) (2016) 4025–4031.
[6] C. Wang, E. Gao, L. Wang, Z. Xu, Mechanics of network materials with responsive crosslinks, C. R. Mec. 342 (5) (2014) 264–272.
[7] X. Wei, M. Naraghi, H.D. Espinosa, Optimal length scales emerging from shear load transfer in natural materials: application to carbon-based nanocomposite design, ACS Nano 6 (3) (2012) 2333–2344.
[8] O.C. Compton, S.W. Cranford, K.W. Putz, Z. An, L.C. Brinson, M.J. Buehler, et al., Tuning the mechanical properties of graphene oxide paper and its associated polymer nanocomposites by controlling cooperative intersheet hydrogen bonding, ACS Nano 6 (3) (2012) 2008–2019.
[9] S. Lin, M.J. Buehler, Thermal transport in monolayer graphene oxide: atomistic insights into phonon engineering through surface chemistry, Carbon 77 (2014) 351–359.
[10] X. Wei, L. Mao, R.A. Soler-Crespo, J.T. Paci, J. Huang, S.T. Nguyen, et al., Plasticity and ductility in graphene oxide through a mechanochemically induced damage tolerance mechanism, Nat. Commun. 6 (2015) 8029.
[11] E. Gao, C. Duan, Z. Xu, Fabricating highly ordered nanofiber assemblies by controlled shear flow and solvent evaporation, 2016 arXiv:1603.07473.
[12] X. Wei, Z. Meng, L. Ruiz, W. Xia, C. Lee, J.W. Kysar, et al., Recoverable slippage mechanism in multilayer graphene leads to repeatable energy dissipation, ACS Nano 10 (2) (2016) 1820–1828.
[13] C. Lee, X. Wei, J.W. Kysar, J. Hone, Measurement of the elastic properties and intrinsic strength of monolayer graphene, Science 321 (5887) (2008) 385–388.
[14] F. Liu, P. Ming, J. Li, Ab initio calculation of ideal strength and phonon instability of graphene under tension, Phys. Rev. B 76 (6) (2007) 064120.
[15] Z. Xu, Graphene nano-ribbons under tension, J. Comput. Theor. Nanosci. 6 (3) (2009) 625–628.
[16] E. Gao, Z. Xu, Thin-shell thickness of two-dimensional materials, J. Appl. Mech. 82 (12) (2015) 121012.
[17] L. Ruiz, W. Xia, Z. Meng, S. Keten, A coarse-grained model for the mechanical behavior of multi-layer graphene, Carbon 82 (2015) 103–115.
[18] C. Chen, Q.-H. Yang, Y. Yang, W. Lv, Y. Wen, P.-X. Hou, et al., Self-assembled free-standing graphite oxide membrane, Adv. Mater. 21 (29) (2009) 3007–3011.
[19] G. Xin, H. Sun, T. Hu, H.R. Fard, X. Sun, N. Koratkar, et al., Large-area free-standing graphene paper for superior thermal management, Adv. Mater. 26 (26) (2014) 4521–4526.
[20] Z. Liu, Z. Li, Z. Xu, Z.X. Xia, X.Z. Hu, L. Kou, et al., Wet-spun continuous graphene films, Chem. Mater. 26 (23) (2014) 6786–6795.
[21] M. Zhang, Y. Wang, L. Huang, Z. Xu, C. Li, G. Shi, Multifunctional pristine chemically modified graphene films as strong as stainless steel, Adv. Mater. 27 (42) (2015) 6708–6713.
[22] Z. Xu, C. Gao, Graphene chiral liquid crystals and macroscopic assembled fibres, Nat. Commun. 2 (2011) 571.
[23] S. Park, K.S. Lee, G. Bozoklu, W. Cai, S.T. Nguyen, R.S. Ruoff, Graphene oxide papers modified by divalent ions-enhancing mechanical properties via chemical cross-linking, ACS Nano 2 (3) (2008) 572–578.
[24] N.V. Medhekar, A. Ramasubramaniam, R.S. Ruoff, V.B. Shenoy, Hydrogen bond networks in graphene oxide composite paper: structure and mechanical properties, ACS Nano 4 (4) (2010) 2300–2306.
[25] ASTM D882-12, Standard Test Method for Tensile Properties of Thin Plastic Sheeting, ASTM International, West Conshohocken, PA, 2012. http://www.astm.org.
[26] L.J. Bonderer, A.R. Studart, L.J. Gauckler, Bioinspired design and assembly of platelet reinforced polymer films, Science 319 (5866) (2008) 1069–1073.
[27] K. Chen, B. Shi, Y. Yue, J. Qi, L. Guo, Binary synergy strengthening and toughening of bio-inspired nacre-like graphene oxide/sodium alginate composite paper, ACS Nano 9 (8) (2015) 8165–8175.
[28] Q. Cheng, M. Wu, M. Li, L. Jiang, Z. Tang, Ultratough artificial nacre based on conjugated cross-linked graphene oxide, Angew. Chem. Int. Ed. 52 (13) (2013) 3750–3755.
[29] W. Cui, M. Li, J. Liu, B. Wang, C. Zhang, L. Jiang, et al., A strong integrated strength and toughness artificial nacre based on dopamine cross-linked graphene oxide, ACS Nano 8 (9) (2014) 9511–9517.
[30] T. Gong, D.V. Lam, R. Liu, S. Won, Y. Hwangbo, S. Kwon, et al., Thickness dependence of the mechanical properties of free-standing graphene oxide papers, Adv. Funct. Mater. 25 (24) (2015) 3756–3763.
[31] L. Huang, C. Li, W. Yuan, G. Shi, Strong composite films with layered structures prepared by casting silk fibroin-graphene oxide hydrogels, Nanoscale 5 (9) (2013) 3780–3786.
[32] S. Huang, S.L. Phua, W. Liu, G. Ding, X. Lu, Nacre-like composite films based on mussel-inspired 'glue' and nanoclay, RSC Adv. 4 (3) (2014) 1425–1431.
[33] R. Jalili, S.H. Aboutalebi, D. Esrafilzadeh, K. Konstantinov, S.E. Moulton, J.M. Razal, et al., Organic solvent-based graphene oxide liquid crystals: a facile route toward the next generation of self-assembled layer-by-layer multifunctional 3D architectures, ACS Nano 7 (5) (2013) 3981–3990.
[34] Y.Q. Li, T. Yu, T.Y. Yang, L.X. Zheng, K. Liao, Bio-inspired nacre-like composite films based on graphene with superior mechanical, electrical, and biocompatible properties, Adv. Mater. 24 (25) (2012) 3426–3431.
[35] M. Lian, J. Fan, Z. Shi, S. Zhang, H. Li, J. Yin, Gelatin-assisted fabrication of graphene-based nacre with high strength, toughness, and electrical conductivity, Carbon 89 (0) (2015) 279–289.
[36] J. Liang, Y. Huang, L. Zhang, Y. Wang, Y. Ma, T. Guo, et al., Molecular-level dispersion of graphene into poly(vinyl alcohol) and effective reinforcement of their nanocomposites, Adv. Funct. Mater. 19 (14) (2009) 2297–2302.
[37] J.Y. Oh, Y.S. Kim, Y. Jung, S.J. Yang, C.R. Park, Preparation and exceptional mechanical properties of bone-mimicking size-tuned graphene oxide@carbon nanotube hybrid paper, ACS Nano 10 (2) (2016) 2184–2192.
[38] B.S. Shim, J. Zhu, E. Jan, K. Critchley, S. Ho, P. Podsiadlo, et al., Multiparameter structural optimization of single-walled carbon nanotube composites: toward record strength, stiffness, and toughness, ACS Nano 3 (7) (2009) 1711–1722.
[39] Z. Tan, M. Zhang, C. Li, S. Yu, G. Shi, A general route to robust nacre-like graphene oxide films, ACS Appl. Mater. Interfaces 7 (27) (2015) 15010–15016.
[40] S. Wan, Y. Li, J. Peng, H. Hu, Q. Cheng, L. Jiang, Synergistic toughening of graphene oxide-molybdenum disulfide-thermoplastic polyurethane ternary artificial nacre, ACS Nano 9 (1) (2015) 708–714.
[41] J. Wang, Q. Cheng, L. Lin, L. Jiang, Synergistic toughening of bioinspired poly(vinyl alcohol)-clay-nanofibrillar cellulose artificial nacre, ACS Nano 8 (3) (2014) 2739–2745.
[42] J. Wang, L. Lin, Q. Cheng, L. Jiang, A strong bio-inspired layered pnipam-clay nanocomposite hydrogel, Angew. Chem. Int. Ed. 51 (19) (2012) 4676–4680.
[43] J. Wang, J. Qiao, J. Wang, Y. Zhu, L. Jiang, Bioinspired hierarchical alumina-graphene oxide-poly(vinyl alcohol) artificial nacre with optimized strength and toughness, ACS Appl. Mater. Interfaces 7 (17) (2015) 9281–9286.
[44] X. Wang, H. Bai, Z. Yao, A. Liu, G. Shi, Electrically conductive and mechanically strong biomimetic chitosan/reduced graphene oxide composite films, J. Mater. Chem. 20 (41) (2010) 9032.
[45] Y. Wu, R. Cao, L. Ji, W. Huang, X. Yang, Y. Tu, Synergistic toughening of bio-inspired artificial nacre by polystyrene grafted graphene oxide, RSC Adv. 5 (36) (2015) 28085–28091.
[46] S. Xia, Z. Wang, H. Chen, W. Fu, J. Wang, Z. Li, et al., Nanoasperity: structure origin of nacre-inspired nanocomposites, ACS Nano 9 (2) (2015) 2167–2172.
[47] H.B. Yao, Z.H. Tan, H.Y. Fang, S.H. Yu, Artificial nacre-like bionanocomposite films from the self-assembly of chitosan-montmorillonite hybrid building blocks, Angew. Chem. Int. Ed. 49 (52) (2010) 10127–10131.
[48] M. Zhang, L. Huang, J. Chen, C. Li, G. Shi, Ultratough, ultrastrong, and highly conductive graphene films with arbitrary sizes, Adv. Mater. 26 (45) (2014) 7588–7592.
[49] H. Zhao, Y. Yue, Y. Zhang, L. Li, L. Guo, Ternary artificial nacre reinforced by ultrathin amorphous alumina with exceptional mechanical properties, Adv. Mater. 28 (10) (2016) 2037–2042.
[50] S. Eigler, M. Enzelberger-Heim, S. Grimm, P. Hofmann, W. Kroener, A. Geworski, et al., Wet chemical synthesis of graphene, Adv. Mater. 25 (26)

(2013) 3583–3587.
[51] C.A. Schneider, W.S. Rasband, K.W. Eliceiri, NIH image to ImageJ: 25 years of image analysis, Nat. Methods 9 (7) (2012) 671–675.
[52] W. Xia, L. Ruiz, N.M. Pugno, S. Keten, Critical length scales and strain localization govern the mechanical performance of multi-layer graphene assemblies, Nanoscale 8 (12) (2016) 6456–6462.
[53] Y. Liu, B. Xie, Z. Zhang, Q. Zheng, Z. Xu, Mechanical properties of graphene papers, J. Mech. Phys. Solids 60 (4) (2012) 591–605.
[54] S. Vinod, C.S. Tiwary, L.D. Machado, S. Ozden, J. Cho, P. Shaw, et al., Strain rate dependent shear plasticity in graphite oxide, Nano Lett. 16 (2) (2016) 1127–1131.
[55] A.E.H. Love, A Treatise on the Mathematical Theory of Elasticity, fourth ed., Dover Publications, 2011.

Supplementary Information for

Intrinsic Mechanical Properties of Graphene Oxide Films: Strain Characterization and The Gripping Effects

Enlai Gao[1,+], Yeye Wen[2,+], Yanan Yuan[1], Chun Li[2,*] and Zhiping Xu[1,*]

[1]Applied Mechanics Laboratory, Department of Engineering Mechanics and Center for Nano and Micro Mechanics, Tsinghua University, Beijing 100084, China.

[2]Department of Chemistry, Tsinghua University, Beijing 100084, China.

[+]These two authors contribute equally to this work.

[*]Corresponding authors, electronic addresses:

chunli@mail.tsinghua.edu.cn, xuzp@tsinghua.edu.cn

The Supporting Information Materials contain

- Supplementary Figures and Figure Captions

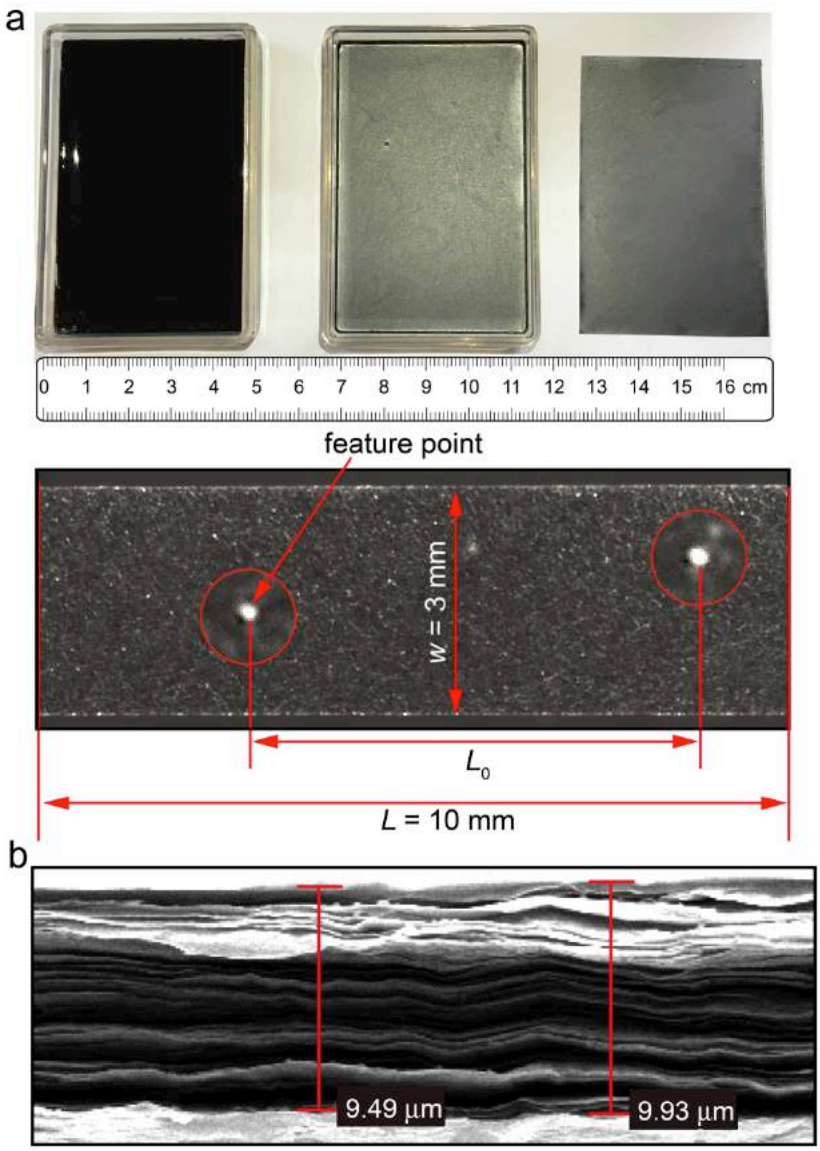

Fig. S1 − (a) GO films fabricated from a dispersion-evaporation procedure, with gauge marks under the magnifying glass. (b) The SEM cross-section micrograph of a GO film.

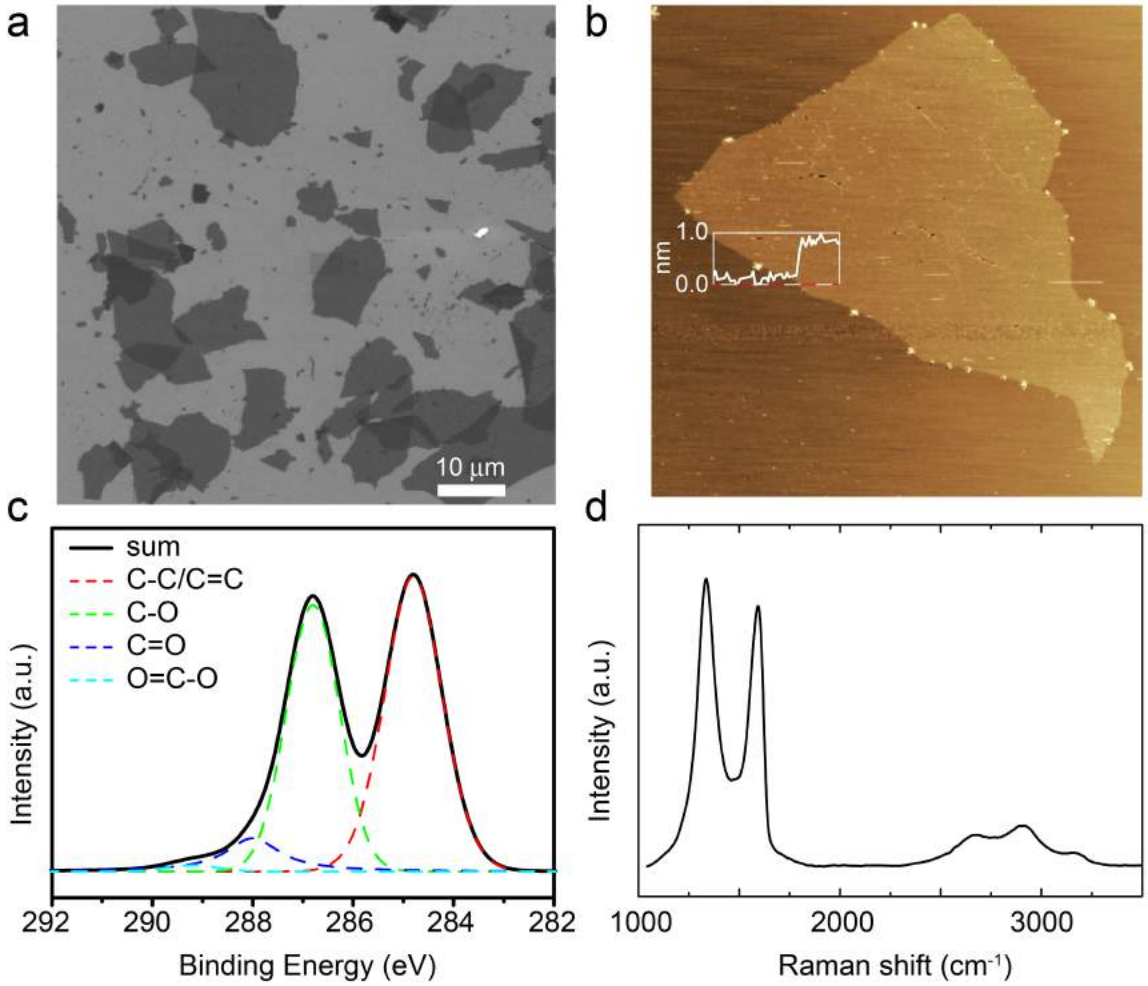

Fig. S2 − Structure characterizations of GO sheets: (a) A SEM image of GO sheets on a deposited on the silicon substrate. (b) The AFM height-profile image of a GO sheet on mica. (c, d) The XPS spectrum and a typical Raman spectrum of GO sheets.

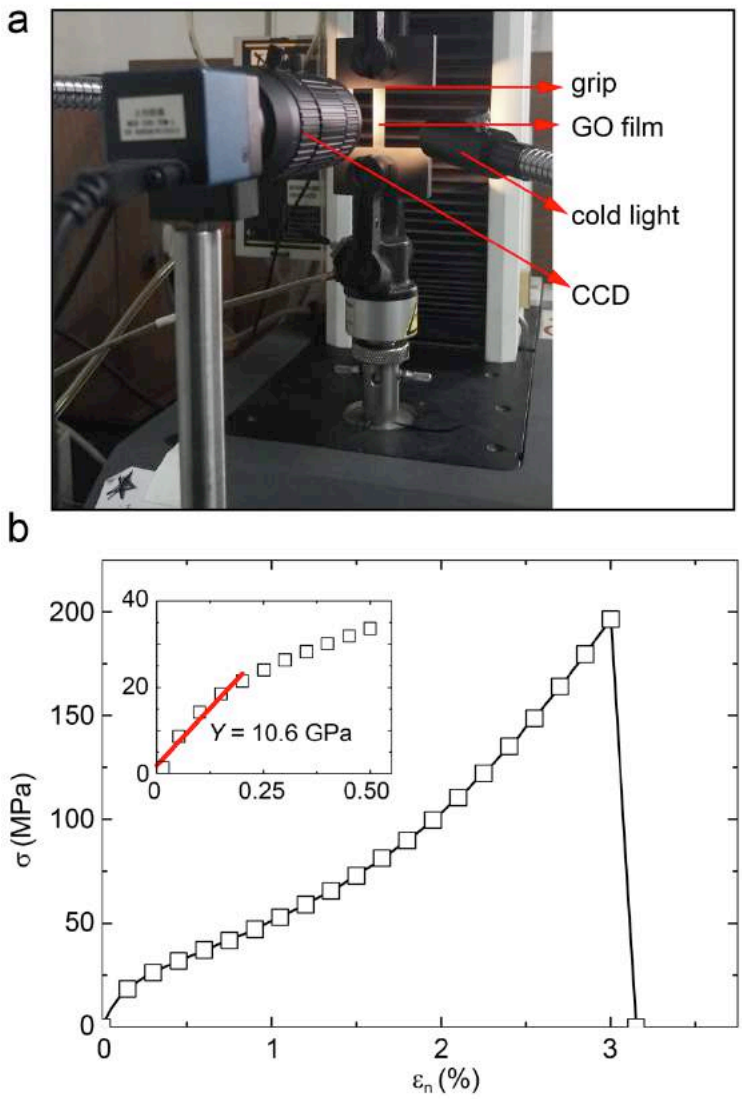

Fig. S3 − (a) The experimental setup for uniaxial tensile tests of GO films. (b) A typical stress-strain curve measured from the experiments.

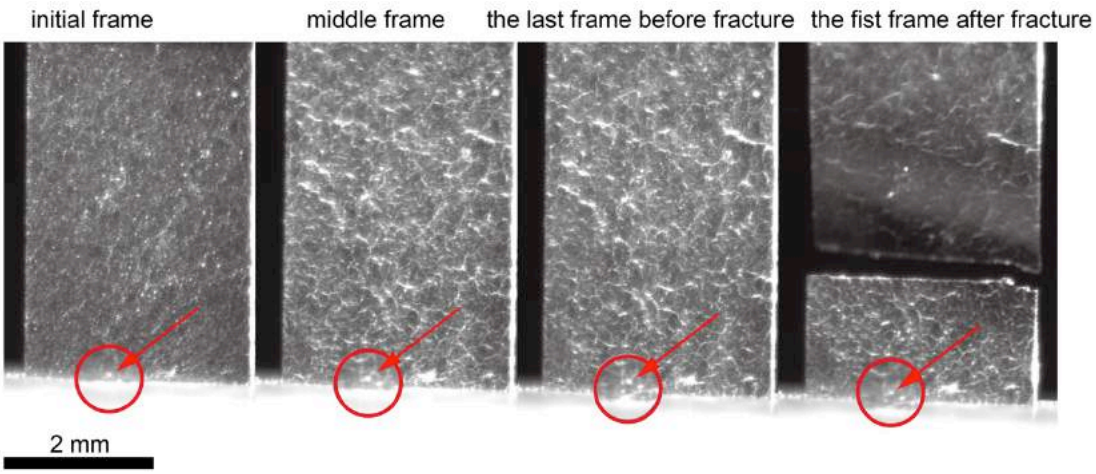

Fig. S4 − Optical images of the GO films under tension, which demonstrate the interfacial slippage at gripping ends and spatially uniform deformation of the whole sample. The shear displacement $s/2$ is 0.115 mm at the highest load in experiments, which is measured from the images by tracking the white dot in red circles.

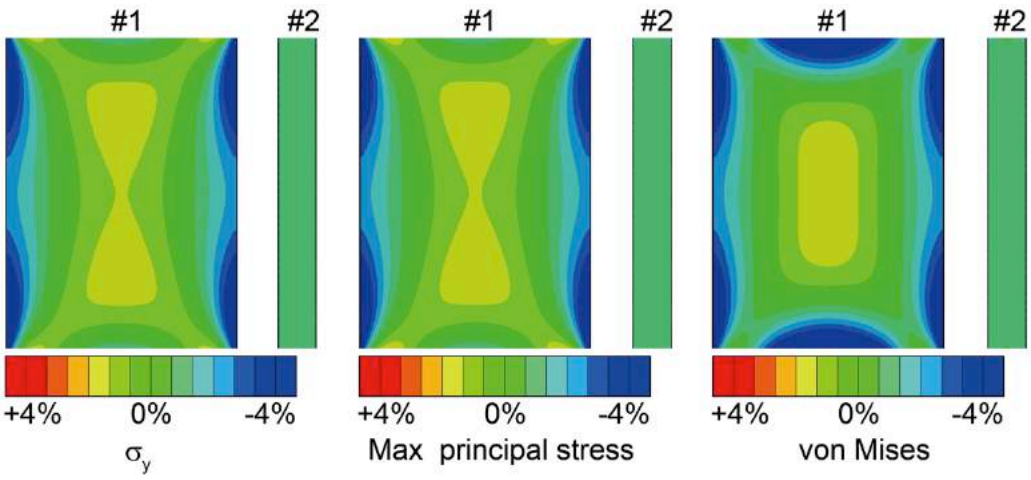

Fig. S5 − In-film stress distribution calculated from the FEA, for the central region of GO samples (80% of the whole length). Analysis was performed for two specimen geometries, which are specimen #1 (5 mm×3 mm) and specimen #2 (30 mm×3 mm). The results show that the maximum derivation from averaged stress is below 5%.

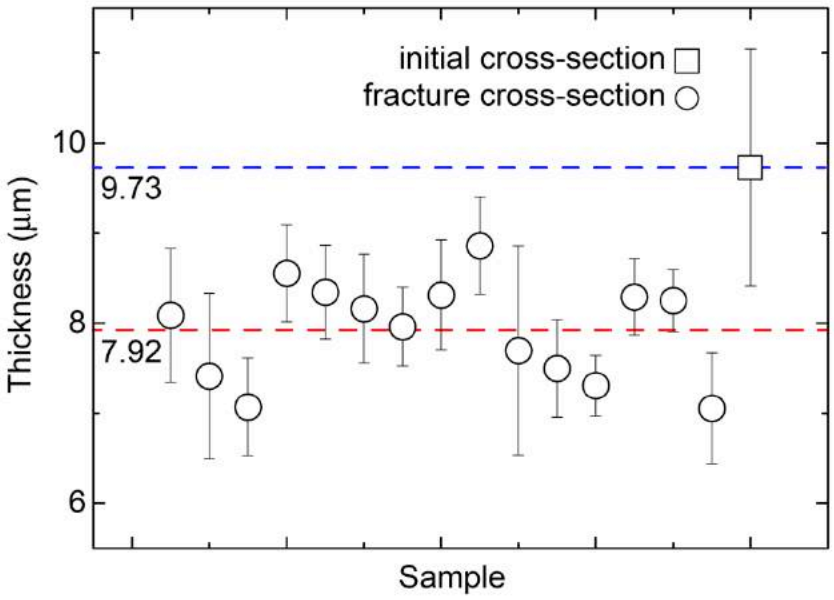

Fig. S6 − The thickness of GO films measured from the cross-section of specimen before being loaded, and after fracture occurs.

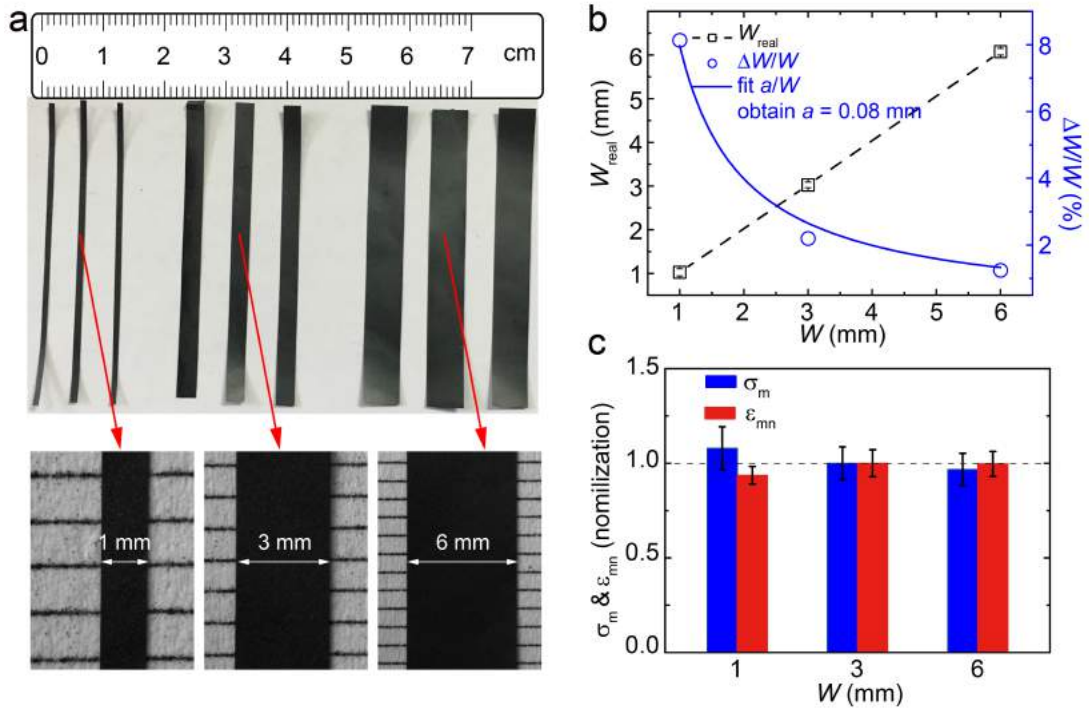

Fig. S7 − (a) Cutted specimens of GO films with widths W of 1, 3 and 6 mm, respectively. (b) Precise measurements of the sample width from CCD show that there are an inaccuracy of ~0.08 mm during the cutting process. (c) Tensile strength and strain to failure measured for samples with different widths. The values are normalized by the data for the sample with W = ~3 mm.